

Numerical stability analysis of solution methods for steady and harmonic balance equations

Original article

Yuxuan Zhang¹, Dingxi Wang^{1,*}

Article history:

Submission date: 11 May 2024

Acceptance date: 28 September 2024

Publication date: 18 February 2025

This is the updated version of a paper originally presented at the Global Power and Propulsion Technical Conference, GPPS Hong Kong23, October 17–19, 2023.



*Correspondence:

DW: dingxi_wang@nwpu.edu.cn

Peer review:

Single blind

Copyright:

© 2025 Zhang and Wang © This is an open access article distributed under the Creative Commons Attribution License (CC-BY 4.0), which permits unrestricted use, distribution, and reproduction in any medium, provided the original work is properly cited and its authors credited.

Keywords:

harmonic balance method; LU-SGS method; block Jacobi method; von Neumann analysis; matrix analysis; numerical stability

Citation:

Zhang Y., Wang D. (2025). Numerical stability analysis of solution methods for steady and harmonic balance equations. *Journal of the Global Power and Propulsion Society*, 9: 1–18.

<https://doi.org/10.33737/jgpps/193865>

¹Northwestern Polytechnical University, 1 Dongxiang Road, Chang'an District, Xi'an, Shaanxi 710129, China

Abstract

This study investigates the stability and convergence properties of solution methods for the steady and unsteady Euler equations. A central scheme with artificial dissipation is used for spatial discretization. A Runge-Kutta scheme is used for the pseudo-time integration. The implicit residual smoothing for steady and harmonic balance solutions is achieved using the Lower-Upper Symmetric Gauss-Seidel(LU-SGS) method and the Lower-Upper Symmetric Gauss-Seidel/Block Jacobi(LU-SGS/BJ) method, respectively. Both the von Neumann and matrix methods are used to analyze the stability of the involved solution methods. The stability of these schemes obtained by the two stability analysis methods is identical for periodic boundary conditions as expected. However, only the matrix method can analyze the stability of solutions involving inlet, outlet, and slip wall boundary conditions. It is found that these boundary conditions enhance the stability of solution methods. Furthermore, the matrix method can also allow for the analysis of the impacts of non-uniformity in grids and flow fields on solution stability. For the harmonic balance equation system, the stability analysis demonstrates that the time spectral source term must be integrated implicitly to avoid instability for analysis with a large maximum grid-reduced frequency. The conclusions can be readily extended to the Reynolds averaged Navier-Stokes equations and verified using a Laval nozzle and the NASA rotor 37.

Introduction

Modern turbomachinery design highly relies on computational fluid dynamics(CFD) for analyzing its performance by solving the steady and unsteady Euler equations or Reynolds-averaged Navier-Stokes(RANS) equations. In numerical analysis, the robustness and the convergence rate of involved solution methods are vitally important for design engineers, as they largely dictate the accomplishment of a design task. Typically, there are two kinds of numerical methods for pseudo-time integration: explicit methods and implicit methods. The representative explicit methods are the multi-stage Runge-Kutta methods (Jameson et al., 1981). Their advantages lie in the low memory consumption, low CPU cost per iteration, and easy implementation. Because of this, they have been very popular in the CFD community. The biggest disadvantage of the explicit methods is their conditional stability. To achieve a stable solution, the time step is limited by the Courant-Fredrichs-Levy (CFL) stability condition. This time step limit is manifested by flow field analysis at off-design conditions and harmonic balance analysis with a large maximum grid-reduced frequency (Hall et al., 2013).

The implicit methods, on the other hand, often have higher memory consumption and higher CPU cost per iteration, and are much more difficult to implement, when compared with the explicit methods. The biggest advantage of the implicit methods is better stability. Thus a much bigger time step can be allowed in an analysis leading to reduced overall time cost. The extended stability of an implicit method depends on the approximation of the system Jacobian matrix. A better approximation generally leads to higher stability but incurs more implementation complexity and computing resources.

The Lower-Upper Symmetric Gauss-Seidel(LU-SGS) method is a popular implicit method, as it represents a good compromise between the advantages and the disadvantages of implicit methods. In a steady analysis, its maximum allowable Courant number is theoretically infinite, though anything more than 1,000 does not make any meaningful difference to the convergence rate of a solution. The LU-SGS method can also be used as a preconditioner for the Runge-Kutta schemes to achieve a better convergence rate and stability (Rossow, 2006).

When it comes to the harmonic balance equation system, the implementation of the LU-SGS method is quite difficult because solutions at different time instants are coupled. To reduce the programming complexity, the Jacobian matrix of the time spectral source term is excluded from the LU-SGS method and it is implicitly integrated using a block Jacobi(BJ) method (Wang and Huang, 2017). Although numerical experiments demonstrate that this decoupled implicit treatment of the time spectral source term can increase solution stability, a thorough stability analysis of this numerical method has not yet been reported in the open literature.

There are two main methods for assessing the stability and the convergence properties of a given numerical scheme. One is well known as the von Neumann method developed by Charney et al. (1950), which has been widely used to analyze the stability of a linear equation system with constant coefficients and periodic boundary conditions. A von Neumann analysis shows that the first-order forward temporal integration scheme is unconditionally unstable for the linearized Burger's equation in the harmonic balance form when a first-order upwind scheme is used for the spatial discretization (Hall et al., 2013). However, the stability of an equation system can be impacted by inlet, outlet, slip wall boundary conditions, and so on. The effect of these boundary conditions on the stability of an equation system can only be analyzed by using the matrix or eigen-analysis method. The Laplace equation and a two-equation model hyperbolic system were examined using the matrix method with various boundary conditions and stretched grids (Roberts and Swanson, 2005). Eriksson and Rizzi (1985) investigated the solution behaviour of a center scheme for two-dimensional Euler equations. The beneficial effects of local time-step scaling and artificial dissipations were studied using an eigen-analysis.

This paper presents the stability analysis results of solution methods for steady and harmonic balance form Euler equations. The solution methods involve a central scheme with blended second- and fourth-order artificial dissipations for the spatial discretization and a Runge-Kutta scheme for pseudo-time integration. The LU-SGS method and LU-SGS/BJ method are used as the implicit residual smoothing for the steady and harmonic balance solutions, respectively. Both the von Neumann and the matrix methods are used to analyze the stability of the involved solution methods. Based on the stability analysis results, the impact of the boundary conditions and the block Jacobi method on solution stability and convergence rate can be analyzed, providing insights on how to obtain a solution fast and robustly. Though the stability analysis is carried out based on the two-dimensional Euler equations, the conclusions can be readily extended to the three-dimensional RANS equations as demonstrated by using a Laval nozzle and the NASA rotor 37.

Methodology

Flow governing equations

The unsteady Euler equations for an ideal gas in a two-dimensional Cartesian coordinate system have been used in the investigation. They are written in a conservative and differential form as

$$\frac{\partial Q}{\partial t} + \frac{\partial F}{\partial x} + \frac{\partial G}{\partial y} = 0 \quad (1)$$

where

$$Q = \begin{pmatrix} \rho \\ \rho u \\ \rho v \\ \rho e_t \end{pmatrix}, F = \begin{pmatrix} \rho u \\ \rho uu + p \\ \rho vu \\ \rho h_t u \end{pmatrix}, G = \begin{pmatrix} \rho v \\ \rho uv \\ \rho vv + p \\ \rho h_t v \end{pmatrix}$$

Q is the conservative variable vector and F, G are convective flux vectors in x and y directions, respectively. p, ρ, u, v, e_t, h_t denote pressure, density, velocity components, total energy, and total enthalpy. For a perfect gas

$$e_t = \frac{p}{(\gamma - 1)\rho} + \frac{1}{2}(u^2 + v^2), h_t = e_t + \frac{p}{\rho}$$

where γ is the ratio of specific heat. The solution of Equation (1) is obtained by using a cell-centered finite volume scheme. The spatial discretization of the equations is achieved using the well-known Jameson–Schmidt–Turbel (JST) scheme (Jameson et al., 1981) together with spectral radius scaled numerical dissipation (Arnone, 1994).

To simplify the following presentation, Equation (1) is rewritten as the following semi-discrete form

$$\Omega \frac{\partial Q}{\partial t} + R(Q) = 0 \tag{2}$$

where Ω denotes the cell volume and $R(Q)$ is the lumped sum of the spatial residual vector, containing the convective contribution $R_c(Q)$ and the artificial dissipative contribution $R_d(Q)$.

Harmonic balance method

The harmonic balance method is a computationally efficient reduced-order technique for time-periodic flows within turbomachinery (Hall et al., 2002). Its analysis time cost can be 1-2 orders of magnitude lower compared with the dual time-stepping method using a whole annulus computational domain for turbomachinery applications. With the harmonic balance method, the time-dependent flow variables are approximated using a truncated temporal Fourier series

$$Q(t) = \bar{Q} + \sum_{n=1}^N [Q_{A,n} \sin(\omega_n t) + Q_{B,n} \cos(\omega_n t)] \tag{3}$$

where \bar{Q} is the vector of time-averaged conservative variables, $Q_{A,n}$, and $Q_{B,n}$ denote the corresponding vectors of Fourier coefficients for the n th harmonic, N is the number of frequency components to be retained in an analysis, and $\omega_n = n\omega$ is the angular frequency of the n th frequency component. For implementation, Equation (3) can be written in a discrete matrix form as

$$Q = D\tilde{Q} \tag{4}$$

where Q is a column vector containing the conservative variable vectors at $2N + 1$ different time instants, \tilde{Q} is the corresponding Fourier coefficient vector. Their definitions are given as follows

$$Q = \begin{pmatrix} Q(t_1) \\ Q(t_2) \\ \vdots \\ Q(t_{2N+1}) \end{pmatrix}, \tilde{Q} = \begin{pmatrix} \bar{Q} \\ Q_{A,1} \\ Q_{B,1} \\ \vdots \\ Q_{A,N} \\ Q_{B,N} \end{pmatrix}$$

and D is given by $D = D \otimes I$, where D is the inverse discrete Fourier transform matrix, \otimes is the Kronecker product, and I is an identity matrix with the size of $n_{\text{var}} \times n_{\text{var}}$. For two-dimensional Euler equations, the number of conservative variables $n_{\text{var}} = 4$. The inverse discrete Fourier transform matrix D is given as

$$D = \begin{pmatrix} 1 & \sin(\omega_1 t_1) & \cos(\omega_1 t_1) & \dots & \sin(\omega_N t_1) & \cos(\omega_N t_1) \\ 1 & \sin(\omega_1 t_2) & \cos(\omega_1 t_2) & \dots & \sin(\omega_N t_2) & \cos(\omega_N t_2) \\ \vdots & \vdots & \vdots & \vdots & \vdots & \vdots \\ 1 & \sin(\omega_1 t_{2N+1}) & \cos(\omega_1 t_{2N+1}) & \dots & \sin(\omega_N t_{2N+1}) & \cos(\omega_N t_{2N+1}) \end{pmatrix} \tag{5}$$

Accordingly the time derivative term of the conservative variable vectors at $2N + 1$ time instants can be approximated by

$$\frac{\partial \mathbf{Q}}{\partial t} = \mathbf{D}_t \tilde{\mathbf{Q}} = \mathbf{D}_t \mathbf{D}_t^{-1} \mathbf{Q} = \mathbf{E} \mathbf{Q} \tag{6}$$

where $\mathbf{D}_t = \mathbf{D}_t \otimes \mathbf{I}$ and \mathbf{D}_t is given by

$$\mathbf{D}_t = \begin{pmatrix} 0 & \omega_1 \cos(\omega_1 t_1) & -\omega_1 \sin(\omega_1 t_1) & \dots & \omega_N \cos(\omega_N t_1) & -\omega_N \sin(\omega_N t_1) \\ 0 & \omega_1 \cos(\omega_1 t_2) & -\omega_1 \sin(\omega_1 t_2) & \dots & \omega_N \cos(\omega_N t_2) & -\omega_N \sin(\omega_N t_2) \\ \vdots & \vdots & \vdots & \vdots & \vdots & \vdots \\ 0 & \omega_1 \cos(\omega_1 t_{2N+1}) & -\omega_1 \sin(\omega_1 t_{2N+1}) & \dots & \omega_N \cos(\omega_N t_{2N+1}) & -\omega_N \sin(\omega_N t_{2N+1}) \end{pmatrix} \tag{7}$$

The matrix \mathbf{E} is defined as the time spectral operator, which turns the physic-time derivative term into the time spectral source term. Substituting Equation (6) into Equation (2), the harmonic balance equation system with a pseudo-time derivative term is given by

$$\Omega \frac{\partial \mathbf{Q}}{\partial \tau} + \Omega \mathbf{E} \mathbf{Q} + \mathbf{R}(\mathbf{Q}) = 0 \tag{8}$$

The pseudo-time derivative term is introduced to facilitate the use of time-marching methods to solve the harmonic balance equations.

Runge-Kutta scheme and LU-SGS method

The time integration is accomplished through a classic four-stage Runge-Kutta scheme together with the LU-SGS method. The LU-SGS method was first proposed by Yoon and Jameson (1988) as a time integration method. It was later used as a residual smoother at each stage of a Runge-Kutta scheme to improve stability and convergence rate (Rossow, 2006). The solution update at the k th stage of a Runge-Kutta scheme is defined as

$$\mathbf{Q}^{(k)} = \mathbf{Q}^{(0)} + \Delta \mathbf{Q}, \quad k = 1, \dots, K \tag{9}$$

where $\mathbf{Q}^{(0)} = \mathbf{Q}^{n-1}$, $\mathbf{Q}^n = \mathbf{Q}^{(K)}$, and $\Delta \mathbf{Q}$ is a column vector containing the solution increment at $2N + 1$ time instants. For the explicit scheme, the solution increment can be obtained directly as follows

$$\Delta \mathbf{Q} = -\alpha_k \sigma \frac{\Delta \tau}{\Omega} [\mathbf{R}(\mathbf{Q}^{(k-1)}) + \Omega \mathbf{E} \mathbf{Q}^{(k-1)}] \tag{10}$$

While the explicit scheme is conditionally stable, the stability and convergence rate of the solution can be further improved by employing the implicit method, the LU-SGS method, as a preconditioner of the Runge-Kutta method. Subsequently, the solution increment is obtained by solving the following equations

$$\left[\mathbf{I} + \varepsilon \sigma \frac{\Delta \tau}{\Omega} \frac{\partial \mathbf{R}}{\partial \mathbf{Q}} \right] \Delta \mathbf{Q} = -\alpha_k \sigma \frac{\Delta \tau}{\Omega} [\mathbf{R}(\mathbf{Q}^{(k-1)}) + \Omega \mathbf{E} \mathbf{Q}^{(k-1)}] \tag{11}$$

where $\partial \mathbf{R} / \partial \mathbf{Q} = \mathbf{I}_{2N+1} \otimes \partial \mathbf{R} / \partial \mathbf{Q}$ is a block diagonal matrix and $\mathbf{I} = \mathbf{I}_{2N+1} \otimes \mathbf{I}$ is an identity matrix. \mathbf{I}_{2N+1} is the identity matrix of size $(2N + 1) \times (2N + 1)$ and $\partial \mathbf{R} / \partial \mathbf{Q}$ is the Jacobian matrix of the residual vector $\mathbf{R}(\mathbf{Q})$, which only contains the contribution of the convective flux for simplification. The pseudo-time step $\Delta \tau$ is calculated by the ratio of a cell volume to the sum of spectral radii of flux Jacobian matrices. In Equation (11), ε denotes the relaxation factor, α_k denotes the k th Runge-Kutta coefficient and σ is the Courant number. The combination of ε , α_k , and σ plays a significant role in determining the stability and damping behavior of a given scheme. Ideally, these coefficients should be optimized by using stability analysis. To solve Equation (11), an approximate LU decomposition is used to replace the left-hand side of the equation, given as follows

$$\mathbf{BLU} \Delta \mathbf{Q} = -\alpha_k \sigma \frac{\Delta \tau}{\Omega} [\mathbf{R}(\mathbf{Q}^{(k-1)}) + \Omega \mathbf{E} \mathbf{Q}^{(k-1)}] \tag{12}$$

here $\mathbf{B} = I_{2N+1} \otimes B$, $\mathbf{L} = I_{2N+1} \otimes L$, and $\mathbf{U} = I_{2N+1} \otimes U$, where B is a scalar, L is the lower operator, and U is the upper operator, given by

$$\begin{aligned}
 B &= 1 + \varepsilon\sigma \frac{\Delta\tau}{\Omega} (r_i + r_j) \\
 L &= I - \varepsilon\sigma \frac{\Delta\tau}{\Omega} (A_i^+ \mathcal{E}_i^{-1} + A_j^+ \mathcal{E}_j^{-1})/B \\
 U &= I + \varepsilon\sigma \frac{\Delta\tau}{\Omega} (A_i^- \mathcal{E}_i^{+1} + A_j^- \mathcal{E}_j^{+1})/B
 \end{aligned}$$

where matrices A_m^+ and A_m^- with m being i or j are defined as follows

$$A_m^+ = \frac{A_m + r_m}{2}, \quad A_m^- = \frac{A_m - r_m}{2}$$

where A_m is the Jacobian matrix of convective flux through a cell face, given as

$$A_m = \frac{\partial F}{\partial Q} S_x + \frac{\partial G}{\partial Q} S_y$$

in which S_x and S_y are the bounding surface projections in the x and y coordinate directions, respectively. r_m is the spectral radius of the Jacobian matrix A_m . The shift operators $\mathcal{E}_i^{\pm l}$ and $\mathcal{E}_j^{\pm l}$ are defined as

$$\mathcal{E}_i^{\pm l} Q_{i,j} = Q_{i\pm l,j}, \quad \mathcal{E}_j^{\pm l} Q_{i,j} = Q_{i,j\pm l}$$

More details about the derivation of the operators BLU can be found in Wang and Huang (2017).

So far the Jacobian matrix of the time spectral source term is not included on the left-hand side of Equation (11), implying that the time spectral source term is integrated explicitly. As the maximum grid-reduced frequency becomes high, the maximum allowable Courant number will be limited or even solution instability can occur in the harmonic balance equation system.

Block Jacobi method

To mitigate the impaired solution stability caused by the time spectral source term, it needs to be integrated implicitly together with other terms as follows

$$\left[I + \varepsilon\sigma \frac{\Delta\tau}{\Omega} \left(\frac{\partial \mathbf{R}}{\partial \mathbf{Q}} + \Omega \mathbf{E} \right) \right] \Delta \mathbf{Q} = -\alpha_k \sigma \frac{\Delta\tau}{\Omega} [\mathbf{R}(\mathbf{Q}^{(k-1)}) + \Omega \mathbf{E} \mathbf{Q}^{(k-1)}] \tag{13}$$

However, the exact inversion of the system Jacobian matrix of $[I + \varepsilon\sigma \Delta\tau/\Omega(\partial \mathbf{R}/\partial \mathbf{Q} + \Omega \mathbf{E})]$ is quite complicated, as \mathbf{E} is a dense matrix. To avoid this complexity, the block Jacobi(BJ) method was proposed by Sicot et al. (2008) to approximately invert the Jacobian matrix of the time spectral source term through iterations. Wang and Huang (2017) combined the block Jacobi method with the LU-SGS method, leading to the LU-SGS/BJ method:

$$\mathbf{BLU} \Delta \mathbf{Q}^m = -\alpha_k \sigma \frac{\Delta\tau}{\Omega} [\mathbf{R}(\mathbf{Q}^{(k-1)}) + \Omega \mathbf{E} \mathbf{Q}^{(k-1)}] - \varepsilon\sigma \Delta\tau \mathbf{E} \Delta \mathbf{Q}^{m-1} \quad m = 1, 2, \dots, M \tag{14}$$

where M is the number of block Jacobi iterations and the initial solution increment $\Delta \mathbf{Q}^0$ is set to 0. At least two Jacobi iterations are required to have the time spectral source term integrated implicitly. The advantage of the block Jacobi method is its easy implementation and minimal alterations to existing codes with a baseline LU-SGS method.

When using the LU-SGS/BJ method to solve the harmonic balance equation system, it is crucial to consider the influence of the time spectral source term in scalar B . Otherwise, the full potential of the LU-SGS/BJ

method cannot be exploited. The scalar B can be modified as follows

$$B = 1 + \varepsilon\sigma \frac{\Delta\tau}{\Omega} (r_i + r_j + N\Omega\omega)$$

where $N\Omega\omega$ is the spectral radius of the time spectral source term.

Boundary conditions

In general, there are four kinds of boundary conditions used in this numerical analysis: subsonic inlet, subsonic outlet, slip wall, and periodic boundary conditions. At a subsonic inlet, the total pressure, total temperature, and flow angle are specified, while the static pressure is extrapolated from the interior domain to the boundary. Additionally, one can also extrapolate the one-dimensional Riemann invariant to the inlet boundary. The Riemann invariant R^- is defined as follows

$$R^- = V - \frac{2c}{\gamma - 1} \quad (15)$$

where V is the velocity magnitude and c is the speed of sound.

The well-posedness of a boundary condition is important for a numerical analysis as it can affect solution convergence characteristics and even solution accuracy. Extrapolating the Riemann invariant at an inlet boundary has been found to offer better convergence properties for nozzle flows (Jameson and Caughey, 2001). Nevertheless, there is currently a lack of stability analysis supporting this conclusion. This paper will examine the better convergence characteristics of extrapolating the Riemann invariant through stability analysis.

At a subsonic outlet boundary, the static pressure is specified, while the density and momentum in the x and y directions are extrapolated from the interior domain to the boundary. To obtain a meaningful unsteady solution for a Laval nozzle and the NASA rotor 37, a sinusoidal static pressure at the outlet is prescribed

$$p = \bar{p} + \Delta p \sin(\omega t) \quad (16)$$

where \bar{p} is the time-averaged static pressure, Δp is the amplitude of static pressure perturbation with the value of $\Delta p = 0.1\bar{p}$, and ω is the angular frequency of unsteadiness.

von Neumann method

Though Swanson et al. (2007) performed a stability analysis of the RK/LU-SGS methods for two-dimensional steady Euler equations, there has been no such effort of the RK/LU-SGS methods for solving the harmonic balance equation system in the open literature. The stability and damping behaviours of the RK/LU-SGS methods will change dramatically due to the time spectral source term in the harmonic balance equation system. To improve the solution stability of a harmonic balance equation system, the block Jacobi method is often used. Therefore, there is also a need to perform a stability analysis of the RK/LU-SGS/BJ method for solving the harmonic balance equation system.

In the von Neumann analysis, we assume the Euler equations are solved in a finite domain with periodic boundary conditions. Let us define a Cartesian grid consisting of $i_m \times j_m$ cells, where the length and width of each cell are denoted by Δx and Δy , respectively. $\mathbf{Q}'_{i,j}$ denotes the numerical error at the cell (i, j) and can be approximated using a truncated spatial Fourier series as follows

$$\mathbf{Q}'_{i,j} = \sum_{n=-i_m}^{i_m} \sum_{m=-j_m}^{j_m} \hat{\mathbf{Q}}_{n,m} e^{J(i\varphi_x + j\varphi_y)} \quad (17)$$

where $J = \sqrt{-1}$ is the imaginary unit and $\hat{\mathbf{Q}}_{n,m}$ is the amplitude of a spatial harmonic. φ_x and φ_y are the phase angles in the x and y directions of the spatial harmonic, covering the range of $[-\pi, \pi]$ respectively.

The numerical error $\mathbf{Q}'_{i,j}$ satisfies the linear form of Equation (14), given as

$$BLU\Delta\mathbf{Q}'_{i,j}{}^m = -\alpha_k\sigma \frac{\Delta\tau}{\Omega} [\mathcal{L} + \Omega E] \mathbf{Q}'_{i,j}{}^{(k-1)} - \varepsilon\sigma\Delta\tau E\Delta\mathbf{Q}'_{i,j}{}^{m-1} \quad (18)$$

where $\mathcal{L} = I_{2N+1} \otimes \mathcal{L}$ is the block diagonal matrix and \mathcal{L} is the linearized discrete residual operator, consisting of the convective part \mathcal{L}_c and dissipative part \mathcal{L}_d as follows

$$\mathcal{L} = \mathcal{L}_c + \mathcal{L}_d \tag{19}$$

As the Cartesian grid is uniform, \mathcal{L}_c and \mathcal{L}_d can be given by

$$\begin{aligned} \mathcal{L}_c &= \frac{\Delta y}{2} [A_F(\mathcal{E}_i^{+1} - \mathcal{E}_i^{-1})] + \frac{\Delta x}{2} [A_G(\mathcal{E}_j^{+1} - \mathcal{E}_j^{-1})] \\ \mathcal{L}_d &= \Lambda_i \varepsilon^{(4)} [\mathcal{E}_i^{+2} - 4\mathcal{E}_i^{+1} + 6 - 4\mathcal{E}_i^{-1} + \mathcal{E}_i^{-2}] I \\ &\quad + \Lambda_j \varepsilon^{(4)} [\mathcal{E}_j^{+2} - 4\mathcal{E}_j^{+1} + 6 - 4\mathcal{E}_j^{-1} + \mathcal{E}_j^{-2}] I \end{aligned}$$

where $A_F = (\partial F / \partial Q)$ and $A_G = (\partial G / \partial Q)$ are the Jacobian matrices of the convective fluxes in the x and y direction. $\varepsilon^{(4)}$ is the linear dissipative coefficient. Λ_i and Λ_j are the modified spectral radii

$$\begin{aligned} \Lambda_i &= \left[1 + \left(\frac{\Lambda_G}{\Lambda_F} \right)^{0.6} \right] \Lambda_F \\ \Lambda_j &= \left[1 + \left(\frac{\Lambda_F}{\Lambda_G} \right)^{0.6} \right] \Lambda_G \end{aligned}$$

in which Λ_F and Λ_G are the spectral radii of the Jacobian matrices A_F and A_G . Substitute a single spatial harmonic $\hat{Q} e^{j(i\varphi_x + j\varphi_y)}$ from Equation (17) into Equation (18), we can obtain

$$B \hat{L} \hat{U} \Delta \hat{Q}^m = -\alpha_k \sigma \frac{\Delta \tau}{\Omega} [\hat{\mathcal{L}} + \Omega E] \hat{Q}^{(k-1)} - \varepsilon \sigma \Delta \tau E \Delta \hat{Q}^{m-1} \tag{20}$$

where $\hat{\mathcal{L}}$ is the transformed linear residual operator, given by

$$\hat{\mathcal{L}} = \hat{\mathcal{L}}_c + \hat{\mathcal{L}}_d \tag{21}$$

where

$$\begin{aligned} \hat{\mathcal{L}}_c &= \frac{\Delta y}{2} [A_F(e^{j\varphi_x} - e^{-j\varphi_x})] + \frac{\Delta x}{2} [A_G(e^{j\varphi_y} - e^{-j\varphi_y})] \\ \hat{\mathcal{L}}_d &= \Lambda_i \varepsilon^{(4)} [e^{2j\varphi_x} - 4e^{j\varphi_x} + 6 - 4e^{-j\varphi_x} + e^{-2j\varphi_x}] \\ &\quad + \Lambda_j \varepsilon^{(4)} [e^{2j\varphi_y} - 4e^{j\varphi_y} + 6 - 4e^{-j\varphi_y} + e^{-2j\varphi_y}] \end{aligned}$$

and \hat{L} and \hat{U} are the transformed lower and upper operators, given by

$$\begin{aligned} \hat{L} &= 1 - \varepsilon \sigma \frac{\Delta \tau}{\Omega} (\Delta y A_F^+ e^{-j\varphi_x} + \Delta x A_G^+ e^{-j\varphi_y}) / B \\ \hat{U} &= I + \varepsilon \sigma \frac{\Delta \tau}{\Omega} (\Delta y A_F^- e^{j\varphi_x} + \Delta x A_G^- e^{j\varphi_y}) / B \end{aligned}$$

Through M Jacobian iterations, the transformed increment of the solution can be simplified as

$$\Delta \hat{Q} = -\alpha_k \sigma \frac{\Delta \tau}{\Omega} \hat{P} [\hat{\mathcal{L}} + \Omega E] \hat{Q}^{(k-1)} \tag{22}$$

where \hat{P} is the transformed preconditioner. For the LU-SGS/BJ method,

$$\hat{P} = \hat{P}^M$$

which can be obtained as follows

$$\hat{P}^m = \hat{P}_{LU}(\mathbf{I} - \varepsilon\sigma\Delta\tau\Omega\mathbf{E}\hat{P}^{m-1}), \quad m = 1, 2, \dots, M$$

in which the initial value \hat{P}^0 is set to 0. \hat{P}_{LU} is the transformed preconditioner of the LU-SGS method, given by

$$\hat{P}_{LU} = (\mathbf{B}\hat{\mathbf{L}}\hat{\mathbf{U}})^{-1}$$

When $M = 1$, the preconditioner $\hat{P} = \hat{P}_{LU}$, meaning that only the LU-SGS method is applied. When $M \geq 2$ the block Jacobi method is applied to deal with the time spectral source term implicitly. As the K -stage Runge-Kutta method is used for pseudo-time integration, the updated numerical error in the next pseudo-time step can be written as

$$\hat{Q}^n = \mathbf{G}_{RK}\hat{Q}^{n-1} \tag{23}$$

where the amplification matrix \mathbf{G}_{RK} is given by

$$\mathbf{G}_{RK} = \mathbf{I} + \sum_{k=1}^K \alpha_k \dots \alpha_{K-k+1} \mathbf{Z}^k \tag{24}$$

in which \mathbf{Z} is the Fourier symbol of the spatial operator, defined by

$$\mathbf{Z} = -\sigma \frac{\Delta\tau}{\Omega} \hat{P}[\hat{\mathcal{L}} + \Omega\mathbf{E}] \tag{25}$$

Typically, the Fourier symbol \mathbf{Z} is complex. When the phase angles φ_x and φ_y vary from $-\pi$ to π , the Fourier symbol forms a locus on the complex plane. The locus will scale up with an increase in the Courant number or a decrease in the relaxation factor. The magnitude contour of the amplification factor can also be plotted on the complex plane according to Equation (24) with the contour level ranging from 0 to 1. The contour lines, often referred to as the stability region, depend on Runge-Kutta coefficients. The amplification factor measures the growth of the numerical error over iteration. For a stable scheme, the numerical error must not grow with iteration. So the maximum modulus of the amplification factor must be less than or equal to one for all phase angles φ_x and φ_y varying from $[-\pi, \pi]$. In other words, the locus of the Fourier symbol \mathbf{Z} in the complex plane should be inside the stability region of the Runge-Kutta scheme. The maximum allowable Courant number and the minimum allowable relaxation factor thus depend on the interval between the locus of the Fourier symbol and stability domain along the imaginary axis as well as the negative real axis.

Matrix method

The matrix method, also known as the eigenvalue analysis, is a more general approach to stability analysis. It allows for considering various boundary conditions, grid nonuniformities and flow field nonuniformities. In the case of a non-uniform mesh, the total residual function $R(Q)$ for each control volume consists of two parts: the convective part $R_c(Q)$ and the artificial dissipative part $R_d(Q)$. They are expressed as follows

$$\begin{aligned} R_c(Q) &= [F_{\text{con},i+(1/2),j} - F_{\text{con},i-(1/2),j}] + [F_{\text{con},i,j+(1/2)} - F_{\text{con},i,j-(1/2)}] \\ R_d(Q) &= [D_{i+(1/2),j} - D_{i-(1/2),j}] + [D_{i,j+(1/2)} - D_{i,j-(1/2)}] \end{aligned} \tag{26}$$

where the convective fluxes through a bounding surface with the index $i + (1/2)$, omitting the index j , are defined by

$$F_{\text{con},i+(1/2)} = [F \times S_x + G \times S_y]_{i+(1/2)} \tag{27}$$

Fluxes at a bounding surface are calculated by simply averaging their values on two sides of the bounding surface. For example, $F_{i+(1/2)} = 1/2(F_i + F_{i+1})$. The artificial dissipative fluxes are given by

$$D_{i+(1/2)} = \Lambda_{i+(1/2)}[\varepsilon_{i+(1/2)}^{(2)}(Q_{i+1} - Q_i) - \varepsilon_{i+(1/2)}^{(4)}(Q_{i+2} - 3Q_{i+1} + 3Q_i - Q_{i-1})] \tag{28}$$

where $\Lambda_{i+(1/2)} = (1/2)(\Lambda_i + \Lambda_{i+1})$, and $\varepsilon^{(2)}$, $\varepsilon^{(4)}$ are the coefficients of the nonlinear and linear dissipative terms, respectively. The nonlinear dissipative term is designed to provide dissipation at discontinuities such as a shock wave. The linear one is used to suppress spurious solutions, leading to a fast convergence to a steady state. The coefficients $\varepsilon^{(2)}$ and $\varepsilon^{(4)}$ depend on the distribution of static pressure from a solution and the constant parameters $k^{(2)}$ and $k^{(4)}$ (Jameson et al., 1981).

In the stability analysis based on the matrix method, the solution iteration needs to be written in a matrix form. For an explicit scheme, the solution increment is given by

$$\Delta Q_{i,j} = -\alpha_k \sigma \frac{\Delta \tau_{i,j}}{\Omega_{i,j}} [R_{i,j}(Q^{(k-1)}) + \Omega_{i,j} E Q_{i,j}^{(k-1)}] \tag{29}$$

where the index $i = 1, 2, \dots, i_m$ and $j = 1, 2, \dots, j_m$. The matrix form of Equation (29) can be written as follows

$$\begin{pmatrix} \Delta Q_{1,1} \\ \Delta Q_{2,1} \\ \vdots \\ \Delta Q_{i_m,1} \\ \Delta Q_{1,2} \\ \vdots \\ \Delta Q_{i_m,j_m} \end{pmatrix} = -\alpha_k \sigma \begin{pmatrix} \frac{\Delta \tau_{1,1}}{\Omega_{1,1}} I & & & \\ & \ddots & & \\ & & \ddots & \\ & & & \frac{\Delta \tau_{i_m,j_m}}{\Omega_{i_m,j_m}} I \end{pmatrix} \times \left[\begin{pmatrix} R_{1,1}(Q^{(k-1)}) \\ R_{2,1}(Q^{(k-1)}) \\ \vdots \\ R_{i_m,1}(Q^{(k-1)}) \\ R_{1,2}(Q^{(k-1)}) \\ \vdots \\ R_{i_m,j_m}(Q^{(k-1)}) \end{pmatrix} + \begin{pmatrix} \Omega_{1,1} E & & & \\ & \ddots & & \\ & & \ddots & \\ & & & \Omega_{i_m,j_m} E \end{pmatrix} \begin{pmatrix} Q_{1,1} \\ Q_{2,1} \\ \vdots \\ Q_{i_m,1} \\ Q_{1,2} \\ \vdots \\ Q_{i_m,j_m} \end{pmatrix} \right] \tag{30}$$

and here is the short form of Equation (30)

$$\Delta Q^* = -\alpha_k \sigma \left(\frac{\Delta \tau}{\Omega} \right)^* [(R^*)^{(k-1)} + (\Omega E)^* (Q^*)^{(k-1)}] \tag{31}$$

where $(Q^*)^{(k-1)}$ is the solution vector, ΔQ^* represents the solution increment vector, and $(R^*)^{(k-1)}$ is the residual vector containing the convective fluxes and dissipative fluxes at each cell under various boundary conditions. $(\Delta \tau / \Omega)^*$ is a diagonal matrix that contains the ratios of pseudo-time step to volume and $(\Omega E)^*$ is a block diagonal matrix containing the time spectral source terms at each cell. Let us define the column vector Q^* containing the numerical errors at each cell. The numerical error Q^* satisfies the linear equation system, given by

$$\Delta Q^* = -\alpha_k \sigma \left(\frac{\Delta \tau}{\Omega} \right)^* [\mathcal{L}^* + (\Omega E)^*] (Q^*)^{(k-1)} \tag{32}$$

where $\mathcal{L}^* = (\partial R^* / \partial Q^*)$ is the system Jacobian matrix of the total residual R^* , which has been derived manually. In the matrix method, the impact of various boundary conditions on the stability of the solution can be considered as follows.

Firstly, the periodic boundary conditions in the x and y directions are applied in the matrix method, as illustrated in Figure 1a. The use of periodic boundary conditions in the y direction introduces non-zero off-diagonal elements to the system Jacobian matrix \mathcal{L}^* . For the x direction, the periodic boundary condition is implemented in the submatrix along the main diagonal of \mathcal{L}^* . Similarly, this introduces non-zero off-diagonal elements to this

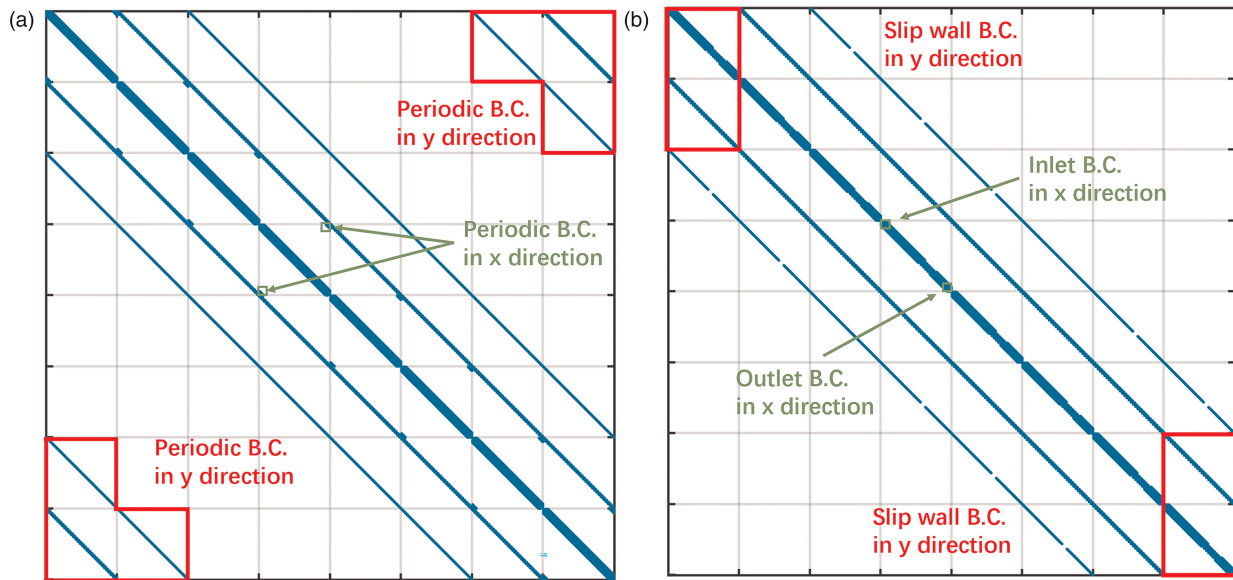


Figure 1. Visualization of the Jacobian matrix of the spatial discrete operator for the 2-D Euler equation system. Nonzero elements are displayed as filled blue dots. (a) Periodic B.C. in x and y directions. (b) Inlet, outlet B.C. in x direction and slip wall B.C. in y direction.

submatrix. The inlet, outlet, and slip wall boundary conditions are taken into account in the stability analysis by modifying relevant off-diagonal elements of \mathcal{L}^* and the submatrix along the diagonal as shown in Figure 1b.

The Jacobian matrix \mathcal{L}^* is usually frozen with an initial or fully converged steady solution. After the Jacobian matrix is given, the updated numerical error at the next pseudo-time step can be written as

$$(Q^{l*})^n = G_{RK}^*(Q^{l*})^{n-1} \tag{33}$$

where G_{RK}^* is the amplification matrix of the equation system, given by

$$G_{RK}^* = I^* + \sum_{k=1}^K \alpha_k \dots \alpha_{k-1} (Z^*)^k \tag{34}$$

where I^* is an identity matrix of size $[n_{var} \cdot i_m \cdot j_m \cdot (2N + 1)] \times [n_{var} \cdot i_m \cdot j_m \cdot (2N + 1)]$ and the transform matrix Z^* is defined as

$$Z^* = -\sigma \left(\frac{\Delta \tau}{\Omega} \right)^* [\mathcal{L}^* + (\Omega E)^*] \tag{35}$$

In the matrix method, if the spectral radius of G_{RK}^* is not larger than one, then the combination of the pseudo-time integration scheme and the spatial discretization scheme will be numerically stable.

Results and discussion

This section presents two different parts. The first part is aimed at investigating the stability of the combination of explicit Runge-Kutta methods with the JST scheme for solving steady and time spectral form Euler equations by using the von Neumann method and the matrix method. The impact of various boundary conditions on solution stability is considered by the matrix method. The second part focuses on the stability analysis of the LU-SGS method for solving the time spectral form 2-D Euler equations and also the stabilization of the block Jacobi method for different grid-reduced frequencies.

The stability of an explicit Runge-Kutta scheme with different boundary conditions

First, the stability of an explicit Runge-Kutta scheme for solving steady Euler equations with periodic boundary conditions is examined using both the von Neumann method and the matrix method. The computational

domain has a length of 0.2 meters and a height of 0.08 meters as shown in Figure 2. It is discretized using a uniform Cartesian grid with 33 points in the x direction and 9 points in the y direction. The resulting grid aspect ratio is $AR = 0.625$. A uniform flow field with a Mach number of $Ma = 0.5$ and a flow angle of $\beta = 0^\circ$ is used as a baseline for linearization. Periodic boundary conditions are assumed in each direction for the von Neumann analysis and matrix analysis. Figure 3 presents the stability analysis results obtained from these two methods.

The locus of the Fourier symbol Z obtained by the von Neumann analysis aligns precisely with the distribution of eigenvalues of the transform matrix Z^* obtained through the matrix method. The good agreement between the two methods verifies the correct implementation of the matrix method. Figure 3 also presents magnitude contours of the amplification factor of the classic four-stage Runge-Kutta scheme with coefficients $\alpha = [1/4, 1/3, 1/2, 1]$. The contour levels are $|G_{RK}| = 0.002, 0.01, 0.05, 0.20, 0.35, 0.50, 0.65, 0.85, 1.00$. The outermost contour corresponds to amplification factors with a magnitude of 1. For a given spatial

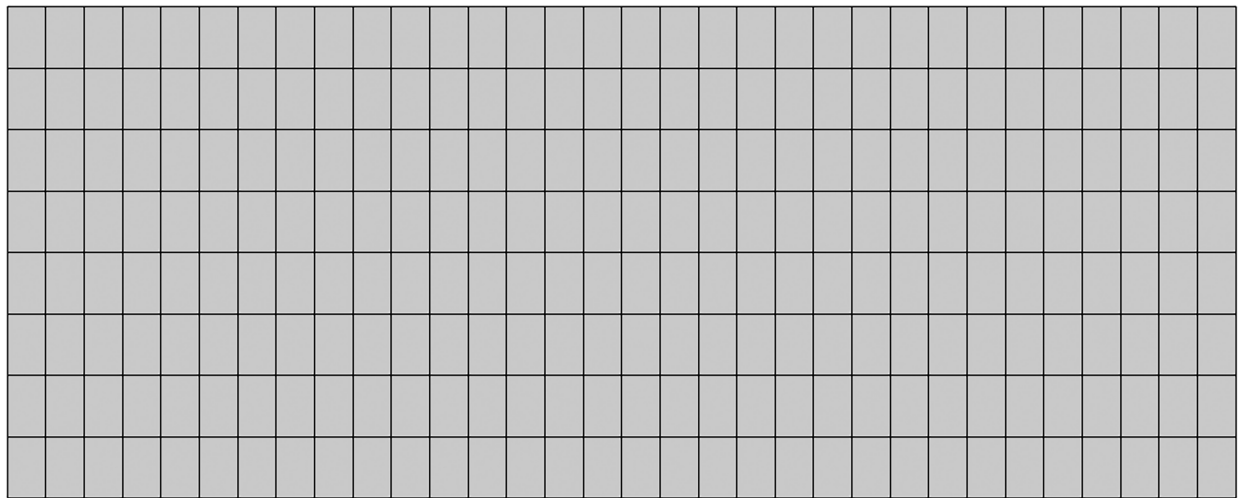


Figure 2. The computational domain and grid for stability analysis.

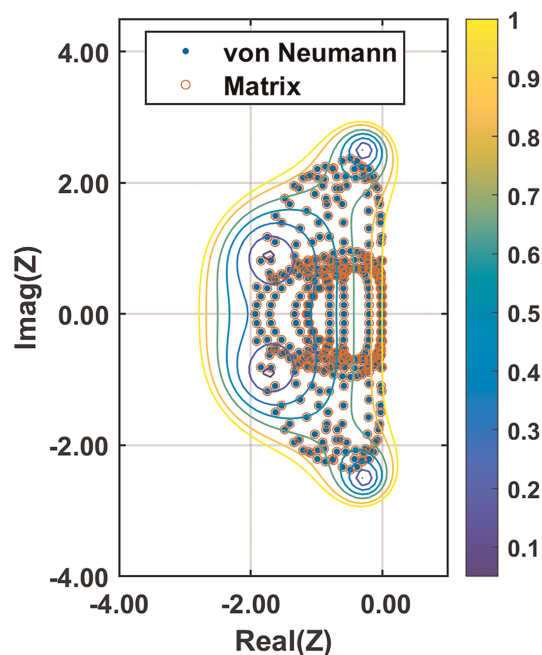


Figure 3. The locus of the Fourier symbol and the eigenvalue spectrum of the transform matrix with periodic boundary conditions, uniform flow fields and grids ($AR = 0.625$, $Ma = 0.5$, $\beta = 0^\circ$, $k^{(4)} = 0.21$, $\sigma = 3$) and the magnitude contours of the amplification factor of the classic four-stage Runge-Kutta scheme.

discretization scheme, the locus of the Fourier symbol or the distribution of the eigenvalues should lie within this outermost contour, referred to as the stability domain. It ensures that the maximum magnitude of the amplification factor is not greater than 1 so that the combination of the pseudo-time integration scheme and the spatial discretization scheme is numerically stable.

To assess the impact of various boundary conditions by the matrix method, these boundary conditions are categorized into four combinations. The first combination serves as a reference, which includes periodic boundary conditions in the x and y directions. The second combination involves inlet and outlet boundary conditions in the x direction and periodic boundary conditions in the y direction. The third combination includes wall boundary conditions in the y direction and periodic boundary conditions in the x directions; The fourth combination consists of inlet and outlet boundary conditions in the x direction and wall boundary conditions in the y direction. The eigenvalue spectra of these four combinations of boundary conditions are presented in Figure 4.

Comparing Figure 4a and b, it can be seen that the inlet and outlet boundary conditions change the distribution of the eigenvalues considerably in the complex plane. Figure 4c presents the eigenvalue spectrum of the third combination, which is quite similar to that in Figure 4a. It implies that the impact of the wall boundary conditions is smaller than that of the inlet and outlet boundary conditions. Figure 4d presents the eigenvalue distribution of the fourth combination, which resembles that of the second one. In conclusion, different combinations of boundary conditions result in varying distributions of eigenvalues in the complex plane, leading to different stability and damping properties. Among these boundary conditions, inlet and outlet boundary conditions have the most significant impact on the eigenvalue spectrum, leading to enhanced stability. Note the impact of boundary conditions diminishes with the increase of grid points.

Next, the impact of different baseline flow fields and inlet boundary conditions on solution stability is investigated by the matrix method. The stability analysis is performed on a Laval nozzle as shown in Figure 5a. A mesh with 65 grid points in the x direction and 17 grid points in the y direction is used to discretize the domain. At the inlet, the total pressure P_t of 101,325 Pa, the total temperature T_t of 288.15 K, and the flow angle of 0° are given. At the outlet, the static pressure P_b of 80,000 Pa is specified. The resulting steady solution is used as the baseline for linearization, as shown in Figure 5b. The flow field is transonic with a shock wave near the throat. The Mach number in front of the shock is 1.5. This indicates a strong non-linearity in the solution.

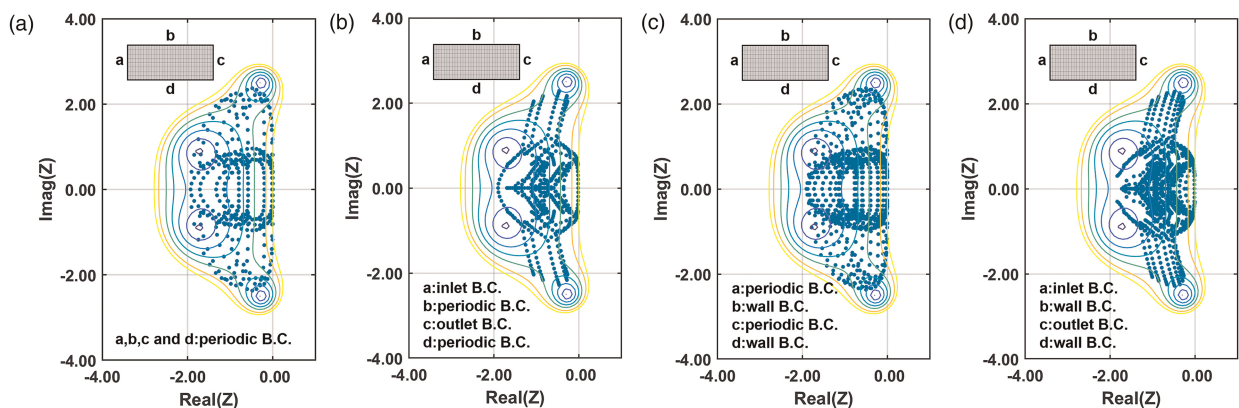


Figure 4. The eigenvalue spectra of the transform matrix for various boundary conditions. ($k^{(4)} = 0.021$, $\sigma = 3$). (a) First combination. (b) Second combination. (c) Third combination. (d) Fourth combination.

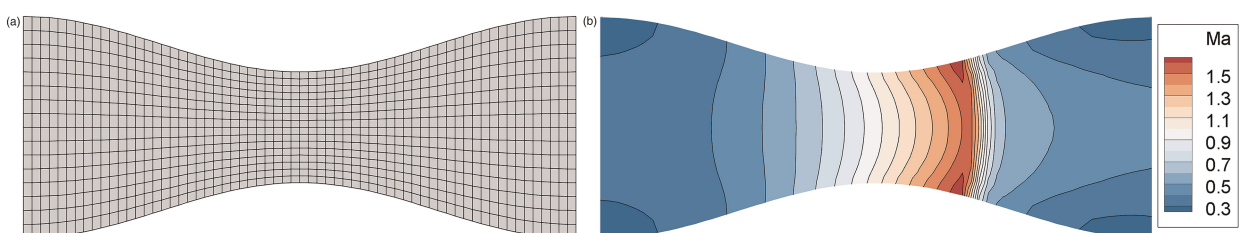


Figure 5. The computational mesh and Mach number contours within a Laval nozzle obtained from solving the 2-D steady Euler equations. (a) mesh. (b) Mach number contour.

The stability analysis results are presented in Figure 6. Figure 6a and b present the eigenvalue spectra of the transform matrix obtained from the uniform flow field and the nozzle flow field with the fourth combination of boundary conditions, respectively. At the inlet boundary, the static pressure is extrapolated, denoted as *inlet1*. When using the steady solution of the nozzle as the baseline, the eigenvalues move along the real axis towards the negative direction, approaching the stability boundary. The resulting stability is reduced. To mitigate the instability caused by the nozzle flow field, the Riemann invariant extrapolation is applied at the inlet, denoted as *inlet2*. Figure 6c shows the eigenvalue spectrum obtained from *inlet2* boundary condition. It can be seen that some leftmost eigenvalues in Figure 6b disappear in Figure 6c, indicating that the Riemann invariant extrapolation improves the solution stability and damping property.

For an unsteady flow analysis using the harmonic balance method, the solution stability is compromised by the time spectral source term. In the von Neumann analysis or the matrix analysis, the time spectral source term introduces a pure imaginary value into the Fourier symbol or the eigenvalues, resulting in a shift of them along the imaginary axis in the complex plane, as illustrated in Figure 7. The extent of this shift is associated with a

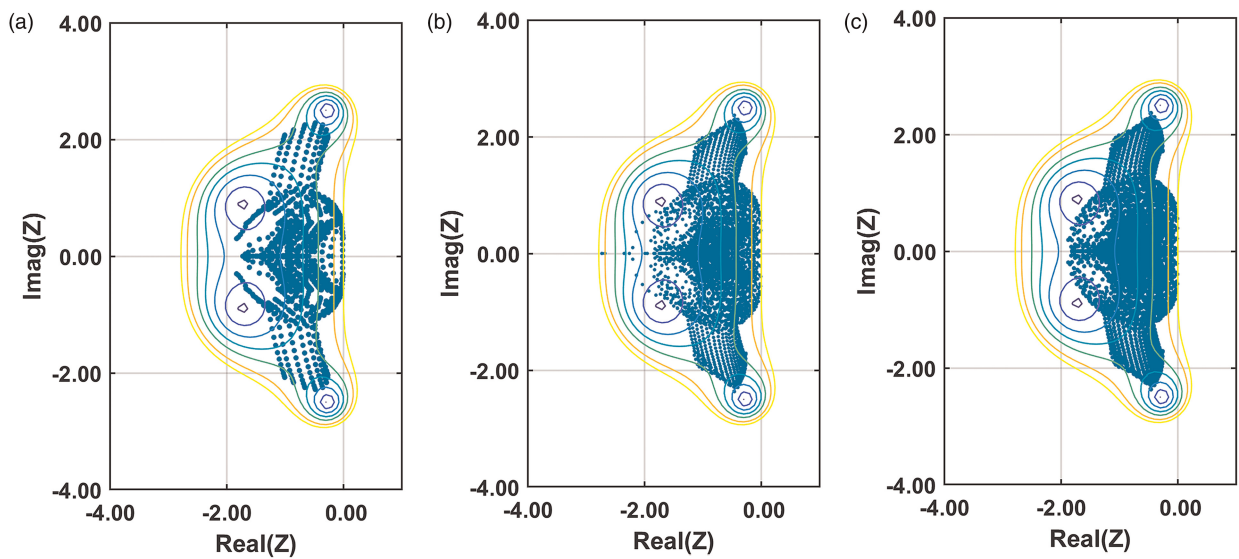


Figure 6. The eigenvalue spectra of the transform matrix for different baseline flow fields and inlet boundary conditions. ($k^{(4)} = 0.021, \sigma = 3$). (a) uniform flow field, inlet1. (b) nozzle flow field, inlet1. (c) nozzle flow field, inlet2.

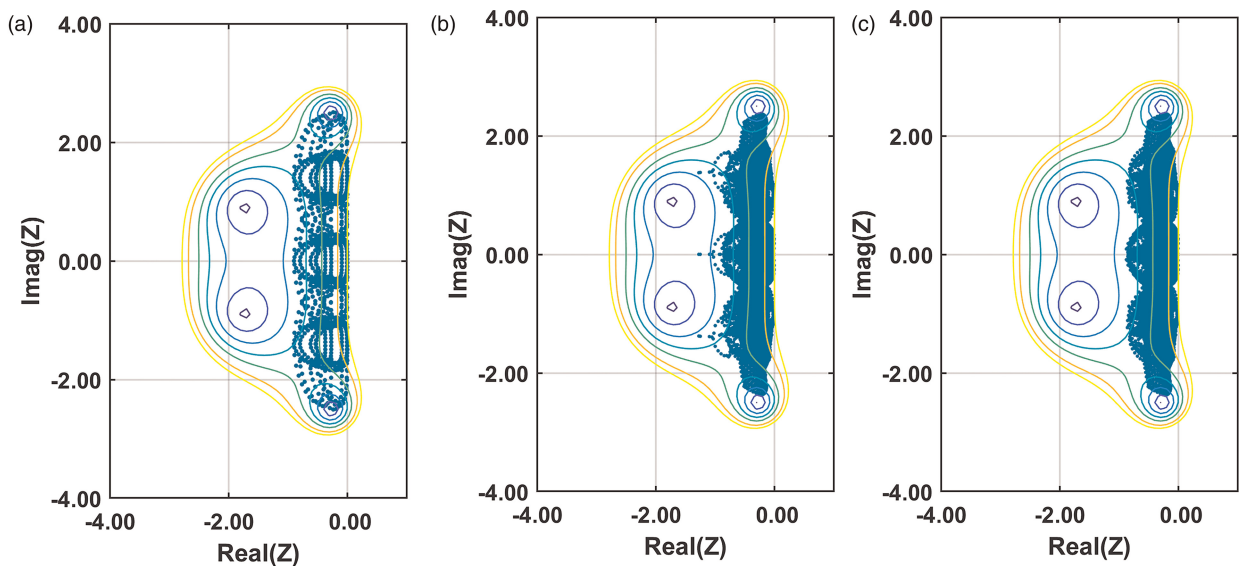


Figure 7. The locus of the Fourier symbol and the eigenvalue spectrum of the transform matrix ($\omega_x = 1, \sigma = 1.4$) and the contours of the magnitude of the amplification in the case of the classic four-stage Runge-Kutta scheme. (a) von Neumann method, periodic. (b) matrix method, inlet1. (c) matrix method, inlet2.

dimensionless parameter, the maximum grid-reduced frequency, defined as

$$\omega_x = \frac{\omega_{\max} \Omega}{r_i + r_j} \quad (36)$$

where ω_{\max} is the maximum angular frequency of the unsteadiness, Ω is the cell volume, r_i and r_j are the spectral radii of the Jacobian matrix of convective fluxes in x and y directions respectively. The maximum grid-reduced frequency is a critical parameter with a substantial impact on the stability of the harmonic balance equation system. If the maximum grid-reduced frequency exceeds a certain value, the resulting locus of the Fourier symbol or the distribution of the eigenvalues will shift outside the stability region. To ensure the stability of the solution, a smaller Courant number has to be used to scale down the eigenvalues so that they stay within the stability domain of the time integration scheme.

To verify the results obtained from the stability analysis, the flow field within the nozzle configuration was analyzed by our in-house solver. A sinusoidal static pressure is prescribed at the outlet. The periodic unsteady flow induced by the pressure perturbation is solved through the harmonic balance method with a single harmonic. The maximum grid-reduced frequency varies from 0 to 8 though altering the frequency of the unsteadiness. Two subsonic inlet boundary conditions, named *inlet1* and *inlet2*, are implemented in the solver. *inlet1* represents the extrapolation of static pressure and *inlet2* represents the extrapolation of the Riemann invariant. When the maximum grid-reduced frequency is set to $\omega_x = 0$, the steady Euler equations are solved. The steady solution reveals that *inlet2* has a higher maximum allowable Courant number than that of *inlet1*, as illustrated in Figure 8. However, the stabilizing effect of *inlet2* does not hold for a harmonic balance solution when the maximum grid-reduced frequency is no less than 1. The results of the numerical experiments agree well with the stability analysis results.

As the maximum grid-reduced frequency increases, the maximum allowable Courant number decreases quickly. Moreover, The maximum allowable Courant numbers with the two different inlet boundary conditions, obtained by numerical experiments, are in good agreement with the matrix analysis results. When it comes to the von Neumann analysis with the assumption of periodic boundary conditions, the predicted maximum allowable Courant numbers are slightly smaller than those obtained by the matrix method at some maximum grid-reduced frequencies, although they are still in good agreement with the results from the numerical experiments.

The stability of the LU-SGS method with the block Jacobi method

The explicit scheme encounters stability issues when it is used to solve the harmonic balance equation, due to the stiffness of the time spectral source term, especially with a large grid-reduced frequency. To stabilize a harmonic balance solution, two implicit methods are presented. The LU-SGS method was first proposed as an implicit preconditioning of the Runge-Kutta method to improve the stability of a steady solution. It can be applied directly to solve the harmonic balance equations without incorporating the Jacobian matrix of the time

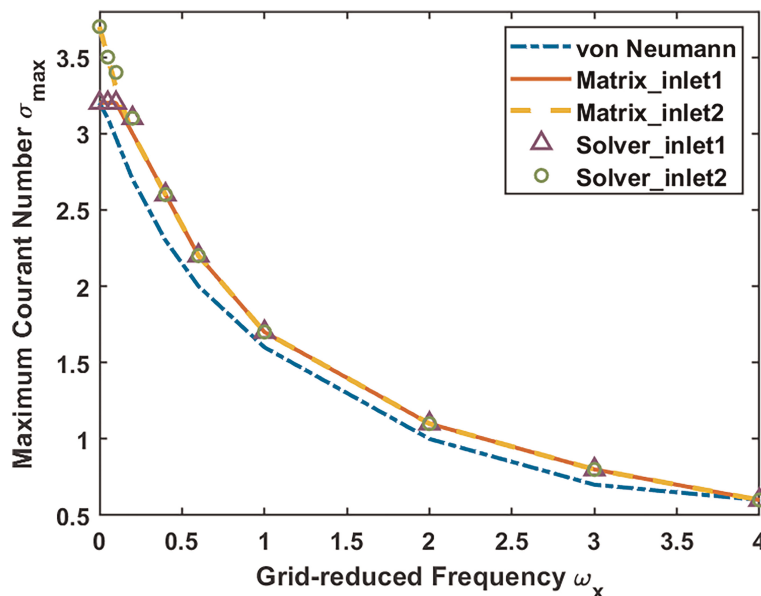


Figure 8. The maximum Courant number varying with the maximum grid-reduced frequency.

spectral source term on the left-hand side. It can also be combined with the Block Jacobi method to integrate the time spectral source term implicitly (Wang and Huang, 2017). To assess the stability of these two implicit methods, a von Neumann analysis is conducted.

In the stability analysis, a uniform flow with a Mach number of 0.5 and a flow angle of 0° is used as the baseline flow for linearization. At first, the stability of the LU-SGS method is investigated for solving the steady Euler equation system (the corresponding grid-reduced frequency $\omega_x = 0$), the Courant number $\sigma = 1000$ and the relaxation factor $\varepsilon = 0.6$. In Figure 9a, the Fourier symbol locus of the LU-SGS method takes a kidney shape in the complex plane, which is notably different from that of the explicit method. In addition, this locus lies within the stability domain of the four-stage Runge-Kutta scheme, even though the Courant number is increased to the order of 10^3 . Therefore, compared to the explicit scheme, the LU-SGS method effectively enhances the stability of a steady solution.

For the harmonic balance equation system, the locus of the Fourier symbol of the LU-SGS method is influenced by the time spectral source term. When the maximum grid-reduced frequency is increased from 0 to 0.2, the locus near the imaginary axis moves to the right side, as shown in Figure 9b. When the maximum grid-reduced frequency reaches 0.5, the locus extends beyond the stability boundary of the classic four-stage Runge-Kutta scheme, shown in Figure 9c. Consequently, the magnitude of the amplification factor is larger than unity and the scheme becomes unstable. To stabilize the solution, the block Jacobi method is used with the LU-SGS method to deal with the time spectral source term implicitly. In Figure 9d, the Fourier symbol locus is restricted within the stability domain when the maximum grid-reduced frequency is set to $\omega_x = 0.5$. Therefore, the LU-SGS/BJ method can effectively stabilize the solution of the harmonic balance equations.

To further examine the stabilization effect of the LU-SGS/BJ method, we consider a sufficiently large maximum grid-reduced frequency in the stability analysis. In Figure 10a, the Fourier symbol locus of the LU-SGS method lies outside the stability domain when the maximum grid-reduced frequency ω_x is set to 2 and the Courant number σ is set to 1,000. However, the locus of the LU-SGS/BJ method is restricted inside the stability domain as shown in Figure 10b. Thus, the LU-SGS/BJ method can effectively stabilize a harmonic balance solution even when the maximum grid-reduced frequency is large, for which the LU-SGS method is unstable.

To verify the stability results obtained through the von Neumann method, the NASA rotor 37 is employed as a more realistic test case. The computational domain consists of one blade passage. The domain is discretized using an H mesh with 57 grid points in the radial direction, 49 grid points in the circumferential direction, and 137 grid points in the streamwise direction, among which 72 grid points are on the blade surface (one side only). At the inlet, the total pressure P_t of 101,811.36 Pa, the total temperature T_t of 288.03 K, and the two flow angles of 0° are given. At the outlet, the back pressure P_b of 115,000 Pa is specified. The 3-D RANS equations, coupled with the Spalart-Allmaras (S-A) turbulence model, are solved by our in-house solver (Wang and Huang, 2017; Huang et al., 2018). The calculated mass flow rate is 20.84 kg/s, the total pressure rate is 1.74 and the isentropic efficiency is 82.72%. The Mach number contours from a steady solution are presented in Figure 11.

Then an unsteady analysis is conducted by varying the static pressure periodically in time at the outlet. The harmonic balance method is used to analyze the unsteady flow with a single harmonic. The maximum grid-reduced frequency varies from 0.2 to 0.5 by altering the frequency of the perturbation. The convergence history

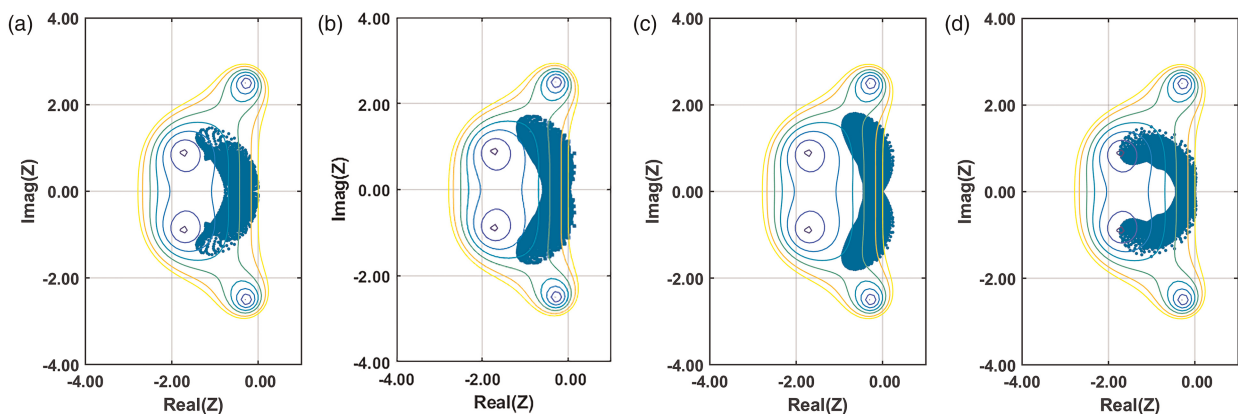


Figure 9. The Fourier symbol loci for different maximum grid-reduced frequencies ($\sigma = 1000$, $\varepsilon = 0.6$) and the magnitude contours of the amplification factor of the classic four-stage Runge-Kutta scheme. (a) $\omega_x = 0$, LU-SGS. (b) $\omega_x = 0.2$, LU-SGS. (c) $\omega_x = 0.5$, LU-SGS. (d) $\omega_x = 0.5$, LU-SGS/BJ.

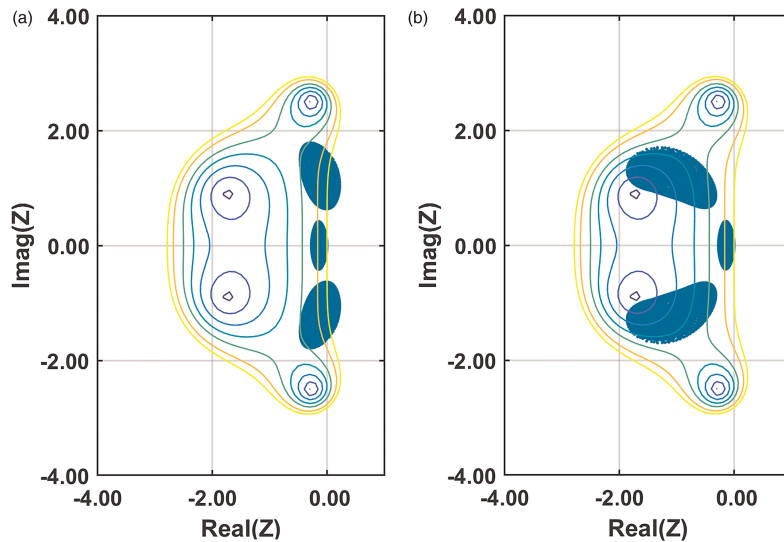


Figure 10. The Fourier symbol loci for $\omega_x = 2$, $\sigma = 1000$, $\varepsilon = 0.6$. (a) LU-SGS method. (b) LU-SGS/BJ method.

of the density equation residual for different implicit methods and maximum grid-reduced frequencies are shown in Figure 12a. Both the LU-SGS and the LU-SGS/BJ method can achieve good convergences when the maximum grid-reduced frequency is not larger than 0.2. However, when the maximum grid-reduced frequency exceeds 0.2, the LU-SGS method fails to achieve convergence with the Courant number of $\sigma = 1000$ and relaxation factor of $\varepsilon = 0.6$. In contrast, the solutions can converge effectively by using the LU-SGS/BJ method. Figure 12b illustrates the time cost comparison between the LU-SGS method and the LU-SGS/BJ method. As expected, the LU-SGS/BJ method requires more CPU time per iteration than that of the LU-SGS method alone. Based on the analysis, we conclude that the block Jacobi method is unnecessary when the maximum grid-reduced frequency is below 0.2. However, if the maximum grid-reduced frequency exceeds this value, the time spectral source term could compromise the stability of the harmonic balance equation system. In such cases, it is recommended to use the block Jacobi method to stabilize the solution so that a larger Courant number can be used to achieve fast convergence.

Furthermore, the numerical experiments of NASA rotor 37 with the maximum grid-reduced frequency of 2 are conducted by increasing the unsteady frequency. The convergence histories of the density equation residual for different implicit methods are shown in Figure 13a. It can be observed that the solution solved with the

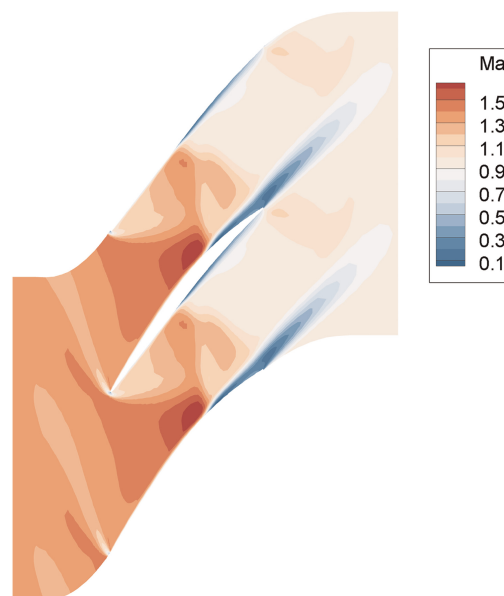


Figure 11. The Mach number contours of the NASA rotor 37 at 50% blade span from the solution of the 3-D steady RANS equation.

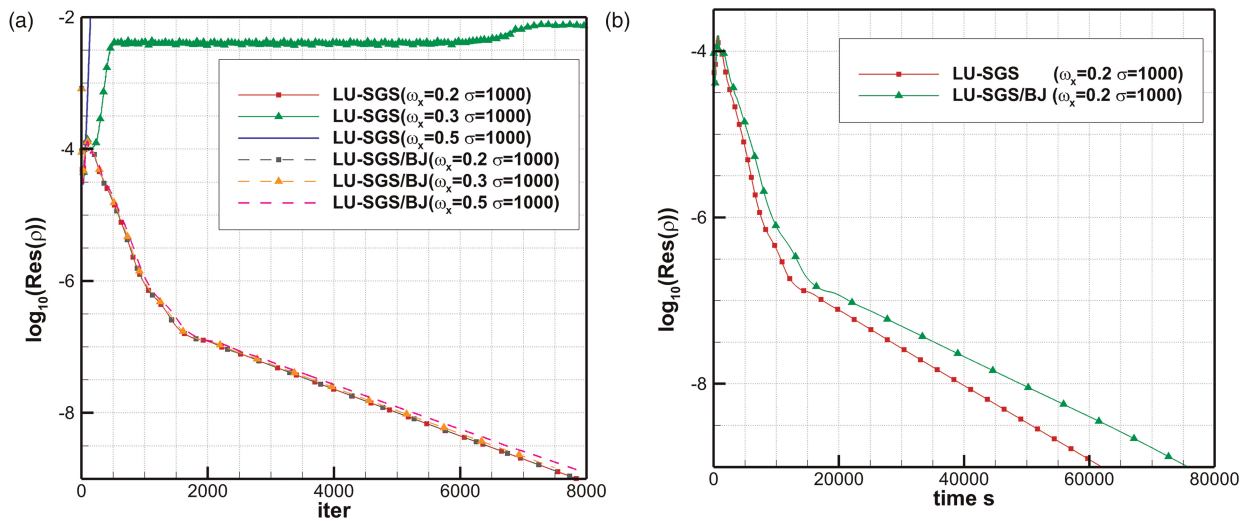


Figure 12. The convergence histories of $Res(p)$ solved using the LU-SGS method and the LU-SGS/BJ method ($\epsilon = 0.6$). (a) iteration. (b) CPU time.

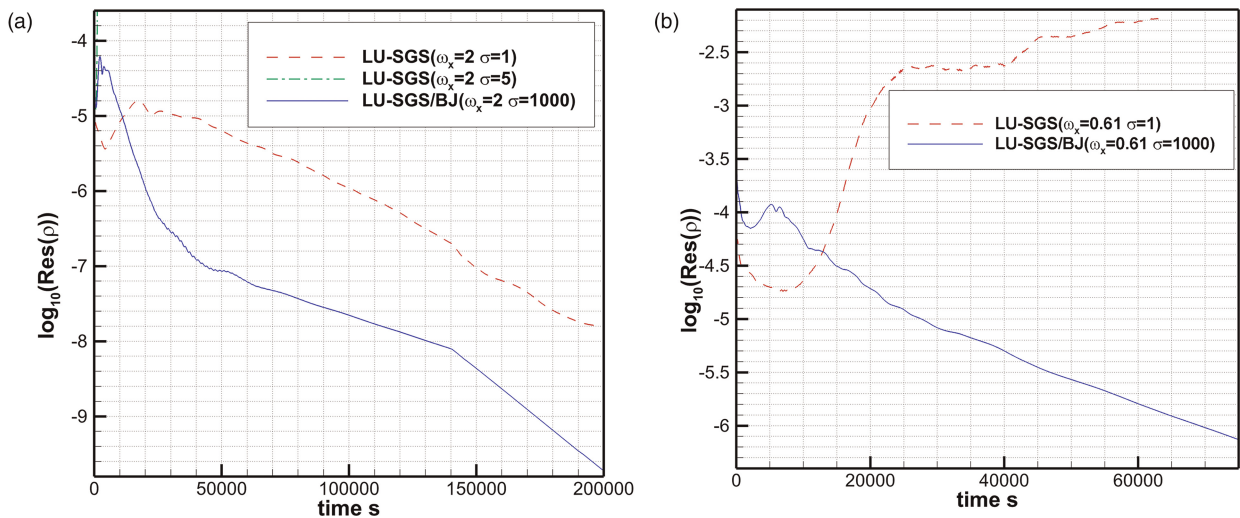


Figure 13. The convergence histories of $Res(p)$ for the LU-SGS method and the LU-SGS/BJ method ($\epsilon = 0.6$). (a) Coarse mesh. (b) Fine mesh.

LU-SGS method can only converge with a very small Courant number, approximately equal to 1. However, with the LU-SGS/BJ method, the maximum Courant number can reach up to 1000, or even higher, resulting in a fast convergence rate. A finer mesh of NASA rotor 37 is employed to confirm the convergence performance. The total number of grid points of the finer mesh is twice that of the coarse mesh. The convergence performance of the LU-SGS/BJ method remains effective, as shown in Figure 13b. Notably, the maximum grid-reduced frequency is reduced due to the reduction in cell volumes of the finer mesh.

The LU-SGS/BJ method demonstrates a significant reduction in total CPU time, requiring approximately 23.5% less time compared to the LU-SGS method to achieve the density equation residual level of 10^{-7} for a coarse mesh. This acceleration is primarily attributed to the better stability of the LU-SGS/BJ method to allow for a much larger Courant number.

Conclusion

In this work, we have investigated the stability of the solution methods for steady and harmonic balance equations by using the von Neumann method and the matrix method. These two approaches show identical stability analysis results of the steady Euler equations with periodic boundary conditions. While the eigenvalue spectrum of the system transform matrix changes dramatically with other boundary conditions such as inlet, outlet, and

slip wall boundary conditions. Furthermore, the matrix method reveals that stability can be improved by using the Riemann invariant extrapolation at an inlet. For the harmonic balance equations, our stability analysis also demonstrates that the time spectral source term leads to a shift along the imaginary axis in the Fourier symbol locus and the eigenvalue spectrum. Consequently, a smaller allowable Courant number is required to ensure a stable solution with an increasing maximum grid-reduced frequency.

To mitigate the impaired solution stability caused by the time spectral source term, the LU-SGS method and the LU-SGS/BJ method are considered in our analysis. In both the von Neumann stability analysis and numerical experiments, the LU-SGS/BJ method can effectively address the stiffness associated with the time spectral source term, while the LU-SGS method fails with a large maximum grid-reduced frequency. Nevertheless, the implementation of the block Jacobi method incurs additional computational costs. To balance stability and computational efficiency, it is recommended that the LU-SGS method alone be used for cases with a maximum grid-reduced frequency $\omega_x \leq 0.2$ and the LU-SGS/BJ method be used for cases with a maximum grid-reduced frequency $\omega_x > 0.2$.

Funding sources

The work is supported by the Science Center for Gas Turbine Project (Project No. P2022-C-II-001-001), the National Natural Science Foundation of China (Grant No. 51976172) and the National Science and Technology Major Project (2017-II-0009-0023).

Competing interests

Yuxuan Zhang declares that he has no conflict of interest. Dingxi wang declares that he has no conflict of interest.

References

- Arnone A. (1994). Viscous analysis of three-dimensional rotor flow using a multigrid method. *Journal of Turbomachinery*. 116 (3): 435–445. <https://doi.org/10.1115/1.2929430>.
- Charney J. G., Fjørtoft R., and von Neumann J. (1950). Numerical integration of the barotropic vorticity equation. *Tellus*. 2 (4): 237–254. <https://doi.org/10.3402/tellusa.v2i4.8607>.
- Eriksson L. E. and Rizzi A. (1985). Computer-aided analysis of the convergence to steady state of discrete approximations to the euler equations. *Journal of Computational Physics*. 57 (1): 90–128. [https://doi.org/10.1016/0021-9991\(85\)90054-3](https://doi.org/10.1016/0021-9991(85)90054-3).
- Hall K. C., Thomas J. P., and Clark W. S. (2002). Computation of unsteady nonlinear flows in cascades using a harmonic balance technique. *AIAA Journal*. 40 (5): 879–886. <https://doi.org/10.2514/2.1754>.
- Hall K. C., Ekici K., Thomas J. P., and Dowell E. H. (2013). Harmonic balance methods applied to computational fluid dynamics problems. *International Journal of Computational Fluid Dynamics*. 27 (2): 52–67. <https://doi.org/10.1080/10618562.2012.742512>.
- Huang X., Wu H., and Wang D. (2018). Implicit solution of harmonic balance equation system using the LU-SGS method and one-step Jacobi/Gauss-Seidel iteration. *International Journal of Computational Fluid Dynamics*. 32 (4–5): 218–232. <https://doi.org/10.1080/10618562.2018.1508658>.
- Jameson A. and Caughey D. (2001). How many steps are required to solve the Euler equations of steady, compressible flow-in search of a fast solution algorithm. In AIAA Paper, 2001–2673, 15th AIAA Computational Fluid Dynamics Conference, Anaheim, CA, USA. <https://doi.org/10.2514/6.2001-2673>.
- Jameson A., Schmidt W., and Turkel E. (1981). Solutions of the Euler equations by finite volume methods using Runge-Kutta time-stepping schemes. In AIAA Paper, 81–1259, 14th AIAA Fluid and Plasma Dynamic Conference, Palo Alto, California. <https://doi.org/10.2514/6.1981-1259>.
- Roberts T. and Swanson R. (2005). A study of multigrid preconditioners using eigensystem analysis. In AIAA Paper, 2005–5229, 17th AIAA Computational Fluid Dynamics Conference, Toronto, Ontario, Canada. <https://doi.org/10.2514/6.2005-5229>.
- Rossov C.-C. (2006). Convergence acceleration for solving the compressible Navier-Stokes equations. *AIAA Journal*. 44 (2): 345–352. <https://doi.org/10.2514/1.15636>.
- Sicot F., Puigt G., and Montagnac M. (2008). Block-Jacobi implicit algorithms for the time spectral method. *AIAA Journal*. 46 (12): 3080–3089. <https://doi.org/10.2514/1.36792>.
- Swanson R. C., Turkel E., and Rossov C.-C. (2007). Convergence acceleration of Runge-Kutta schemes for solving the Navier–Stokes equations. *Journal of Computational Physics*. 224 (1): 365–388. <https://doi.org/10.1016/j.jcp.2007.02.028>.
- Wang D. X. and Huang X. (2017). Solution stabilization and convergence acceleration for the harmonic balance equation system. *Journal of Engineering for Gas Turbines and Power*. 139 (9): 092503–1. <https://doi.org/10.1115/1.4035912>.
- Yoon S. and Jameson A. (1988). Lower-upper symmetric-Gauss-Seidel method for the Euler and Navier-Stokes equations. *AIAA Journal*. 26 (9): 1025–1026. <https://doi.org/10.2514/3.10007>.